

# Calculations of three-nucleon reactions with N<sup>3</sup>LO chiral forces: achievements and challenges

H. Witała, J. Golak, R. Skibiński, and K. Topolnicki

*M. Smoluchowski Institute of Physics,*

*Jagiellonian University, PL-30059 Kraków, Poland*

(Dated: September 29, 2018)

## Abstract

We discuss the application of the chiral N<sup>3</sup>LO forces to three-nucleon reactions and point to the challenges which will have to be addressed. Present approaches to solve three-nucleon Faddeev equations are based on a partial-wave decomposition. A rapid increase of the number of terms contributing to the chiral three-nucleon force when increasing the order of the chiral expansion from N<sup>2</sup>LO to N<sup>3</sup>LO forced us to develop a fast and effective method of automatized partial wave decomposition. At low energies of the incoming nucleon below  $\approx 20$  MeV, where only a limited number of partial waves is required, this method allowed us to perform calculations of reactions in the three-nucleon continuum using N<sup>3</sup>LO two- and three-nucleon forces. It turns out that inclusion of consistent chiral interactions, with relativistic  $1/m$  corrections and short-range  $2\pi$ -contact term omitted in the N<sup>3</sup>LO three-nucleon force, does not explain the long standing low energy  $A_y$ -puzzle. We discuss problems arising when chiral forces are applied at higher energies, where large three-nucleon force effects are expected. It seems plausible that at higher energies, due to a rapid increase of a number of partial waves required to reach convergent results, a three-dimensional formulation of the Faddeev equations which avoids partial-wave decomposition is desirable.

PACS numbers: 21.45.+v, 24.70.+s, 25.10.+s, 25.40.Lw

## I. INTRODUCTION

With the advent of nuclear forces derived in the framework of chiral effective field theory a unique possibility has been offered to study few-nucleon systems and their reactions with consistent two- and many-nucleon interactions. A special place among few-body systems is reserved for the three-nucleon (3N) system, for which mathematically sound theoretical formulation in the form of the Faddeev equations exists, both for bound and scattering states. In last decades numerical algorithms have been developed which allow one to solve numerically Faddeev equations for any dynamical input, containing not only two- but also three-nucleon forces (3NF's) [1, 2].

Using these algorithms and standard, (semi)phenomenological nucleon-nucleon interactions supplemented by model three-nucleon forces, many investigations of the 3N continuum have been done in the past. High precision nucleon-nucleon potentials such as AV18 [3], CD Bonn [4], Nijm I and II [5], which provide a very good description of the nucleon-nucleon data set up to about 350 MeV, have been used. They have been also combined with model 3N forces such as  $2\pi$ -exchange Tucson-Melbourne (TM99) 3NF [6] or Urbana IX model [7].

When realistic NN forces are used to predict binding energies of three-nucleon systems they underestimate the experimental bindings of  ${}^3\text{H}$  and  ${}^3\text{He}$  by about 0.5-1 MeV [8, 9]. This missing binding energy can be restored by introducing a three-nucleon force into the nuclear Hamiltonian [9]. Also the study of elastic nucleon-deuteron (Nd) scattering and nucleon induced deuteron breakup revealed a number of cases where the nonrelativistic description using only pairwise forces is insufficient to explain the data. The best studied case at low energies is the vector analyzing power in elastic nucleon-deuteron scattering for which a large discrepancy exists in the region of its maximum around c.m. angles  $\theta_{c.m.} \approx 125^\circ$  and for incoming nucleon energies below  $\approx 20$  MeV [1, 10]. For the elastic scattering angular distribution at low energies negligible effects of 3NF's have been found and theory based on realistic NN forces agrees well with the data [1, 10].

That picture changes with increasing energy of the three-nucleon system. Generally, the studied discrepancies between experiment and theory using only nucleon-nucleon (NN) potentials become larger and adding a three-nucleon force to the pairwise interactions leads in some cases to a better description of the data. The elastic Nd angular distribution in the region of its minimum and at backward angles is the best known example [11, 12]. The clear discrepancy in these angular regions at energies up to  $\approx 100$  MeV nucleon lab energy between a theory using only NN potentials and the cross section data can be removed by adding a standard models of three-nucleon forces to the nuclear Hamiltonian. Such a 3NF must be adjusted with each NN potential separately to

yield the experimental binding of  ${}^3\text{H}$  and  ${}^3\text{He}$  [10–12]. At energies higher than  $\approx 100$  MeV current three-nucleon forces only partially improve the description of cross section data and the remaining discrepancies, which increase with energy, indicate the possibility of relativistic effects. The need for a relativistic description of three-nucleon scattering was also raised when precise measurements of the total cross section for neutron-deuteron scattering [13] were analyzed within the framework of nonrelativistic Faddeev calculations [14]. Nucleon-nucleon forces alone were insufficient to describe the data above  $\approx 100$  MeV. The effects due to relativistic kinematics considered in [14] at higher energies were comparable in magnitude to the effects due to three-nucleon forces. These results showed the importance of a study taking relativistic effects in the three nucleon continuum into account.

In [15, 16] the first results on relativistic effects in the three-nucleon continuum have been presented. The dynamics was defined by a three-nucleon total momentum zero frame Hamiltonian or mass operator including only pairwise interactions. The mass operator was used to calculate three-nucleon scattering observables. The input to that approach is a “Lorentz boosted” nucleon-nucleon potential, which generates the nucleon-nucleon  $t$ -matrix in a moving frame by solving a standard relativistic Lippmann-Schwinger equation. To get the nucleon-nucleon potential in an arbitrary moving frame one needs the interaction in the two-nucleon total momentum zero frame, which appears in the relativistic nucleon-nucleon Schrödinger or Lippmann-Schwinger equation. The relativistic Schrödinger equation in the two-nucleon total momentum zero frame differs from the nonrelativistic Schrödinger equation just by the relativistic form for the kinetic energy. Current realistic nucleon-nucleon potentials are defined and fit by comparing the solution of the nonrelativistic Schrödinger equation to experimental data. Up to now nucleon-nucleon potentials refitted with the same accuracy in the framework of the relativistic nucleon-nucleon Schrödinger equation do not exist. Such refitting can be, however, avoided by solving a quadratic integral equation whose solution is a relativistic potential which is phase-equivalent to a given input high-precision nonrelativistic nucleon-nucleon potential [17].

In our studies with only nucleon-nucleon interactions we found that when the non-relativistic form of the kinetic energy is replaced by the relativistic one and a proper treatment of the relativistic dynamics is included, the elastic scattering cross section is only slightly increased by relativity at backward angles and higher energies while spin observables are practically unchanged. It is exactly the region of angles and energies where the effects of three-nucleon forces are also significant [10]. These observations prompted us to extend our three-nucleon continuum relativistic Faddeev calculations and include also three-nucleon forces [18]. Again, only small relativistic effects at

higher energies were found for the cross section when 3NF had been included and spin observables remained practically unchanged. It supported conclusions from relativistic calculations performed with 2N forces alone, that for higher energies discrepancies must reflect action of 3NF's.

The main drawback of all those studies was inconsistency between applied NN interactions and 3N forces. In [19] for the first time that inconsistency was removed and low energy 3N continuum investigated with chiral next-to-next-to-leading order ( $N^2LO$ ) NN and 3N forces. The NN interaction in that order, however, does not describe the NN experimental phase-shifts in sufficiently wide energy range to allow application of those forces at higher energies.

In [20] and [21] precise two-nucleon potentials have been developed at next-to-next-to-next-to-leading order ( $N^3LO$ ) of the chiral expansion. They reproduce experimental phase-shifts [22, 23] in a wide energy range and practically with the same high precision as realistic (semi)phenomenological NN potentials. The necessary work to derive the consistent chiral 3NF's at  $N^3LO$  has been done in [24] and [25]. In that order five different topologies contribute to the 3NF. Three of them are of long-range character [24] and are given by two-pion ( $2\pi$ ) exchange graphs, by two-pion-one-pion ( $2\pi-1\pi$ ) exchange graphs, and by the so-called ring diagrams. They are supplemented by the short-range two-pion-exchange-contact ( $2\pi$ -contact) term and by the leading relativistic corrections to the three-nucleon force [25].

Results of refs. [20, 21, 24, 25] enable one now to perform for the first time consistent calculations of three-nucleon reactions at  $N^3LO$  order of chiral expansion. The 3NF at this order does not involve any new unknown low-energy constants (LECs) and depends only on two parameters,  $c_D$  and  $c_E$ , that parametrize the leading one-pion-contact term and the three-nucleon contact term appearing at  $N^2LO$ . Their values need to be fixed at given order from a fit to few-nucleon data. Among the few possible observables that have been used in this connection are the triton binding energy and the neutron-deuteron doublet scattering length  $^2a_{nd}$  [19], the  $^4He$  binding energy, the properties of light nuclei, or the triton  $\beta$  decay rate.

Application of  $N^3LO$  3NF in few-body calculations is challenging due to its very rich and complicated operator structure. The large number of terms in the 3NF at  $N^3LO$  [24, 25] requires an effective method of performing partial-wave decomposition. Recently such a method, which comes under the name of automatized partial-wave decomposition (aPWD) was proposed by us in [26, 27]. In that approach the matrix elements in the 3N momentum-space partial wave basis for different terms contributing to  $N^3LO$  3NF are obtained in two consecutive steps. In the first the spin-momentum and isospin parts of three-nucleon interactions are calculated using a software for symbolic calculations. The resulting momentum-dependent functions are then integrated nu-

merically in five dimensions over angular variables. The major advantage of this method is its generality since it can be applied to any momentum-spin-isospin operator.

In the present paper we would like to present first results obtained with N<sup>3</sup>LO chiral forces and discuss problems which should be resolved in the future. In section II results for low energy elastic neutron-deuteron (nd) scattering will be shown, followed by low energy breakup. In section III we present results and discuss problems encountered at higher energies. To resolve some of those problems and to solve 3N Faddeev equations with NN and 3N chiral forces included it seems that at higher energies three-dimensional approach which avoids partial-wave decomposition is more adequate and in section IV we describe the present state of such an approach. We summarize in section V.

## II. APPLICATION OF N<sup>3</sup>LO CHIRAL FORCES AT LOW ENERGY

### A. Elastic scattering

The nuclear Hamiltonian at N<sup>3</sup>LO order of chiral expansion is fixed by values of LEC's  $c_D$  and  $c_E$ . To determine them we follow ref. [19] and use the experimental triton binding energy  $E^{3H}$  and the nd doublet scattering length  ${}^2a_{nd}$  as two observables from which  $c_D$  and  $c_E$  can be obtained. The procedure can be divided into two steps. First, the dependence of  $E^{3H}$  on  $c_E$  for a given value of  $c_D$  is determined. The requirement to reproduce the experimental value of the triton binding energy yields a set of combinations  $c_D$  and  $c_E$ . This set is then used in the calculations of  ${}^2a_{nd}$ , which allows us to find which pair of  $c_D$  and  $c_E$  describes both observables simultaneously.

We compute the <sup>3</sup>H wave function using the method described in [9], where the full triton wave function  $\Psi = (1 + P)\psi$  is given by its Faddeev component  $\psi$ , which fulfills the Faddeev equation

$$\psi = G_0 t P \psi + (1 + G_0 t) G_0 V^{(1)} (1 + P) \psi. \quad (1)$$

Here  $G_0$  is the free 3N propagator,  $P$  is the permutation operator,  $t$  is the two-body t-matrix generated from a given NN potential through the Lippmann-Schwinger equation, and  $V^{(1)}$  is a part of a 3NF symmetric under the exchange of nucleons 2 and 3.

The doublet scattering length  ${}^2a_{nd}$  is calculated using  $(c_D, c_E)$  pairs, which reproduce the correct value of  $E^{3H}$ . To this end we solve the Faddeev equation for the auxiliary state  $T\phi$  at zero incoming energy [28]

$$T\phi = tP\phi + (1 + tG_0)V^{(1)}(1 + P)\phi + tPG_0T\phi + (1 + tG_0)V^{(1)}(1 + P)G_0T\phi, \quad (2)$$

where the initial channel state  $\phi$  occurring in the driving terms is composed of the deuteron and a plane-wave state of the projectile nucleon. The amplitude for the elastic scattering leading to a corresponding final state  $\phi'$  is then given by

$$\phi'U\phi = \phi'PG_0^{-1}\phi + \phi'PT\phi + \phi'V^{(1)}(1+P)\phi + \phi'V^{(1)}(1+P)G_0T\phi, \quad (3)$$

and for the breakup reaction reads

$$\phi'_0U_0\phi = \phi'_0(1+P)T\phi, \quad (4)$$

where  $\phi'_0$  is the free three-body channel state. We refer to [1] and [2] for a general overview of 3N scattering and for more details on the practical implementation of the Faddeev equations.

In this first preliminary study we restrict the application of N<sup>3</sup>LO 3NF to nd reactions at low energies, with incoming neutron lab. energy below  $\approx 20$  MeV. To get converged results at such energies it is sufficient to include 2N force components with a total two-nucleon angular momenta  $j \leq 3$  in 3N partial-wave states with the total 3N system angular momentum  $J \leq 25/2$ . Including 3NF it is sufficient to incorporate its matrix elements with  $j \leq 3$  and  $J \leq 5/2$ . At those energies the most interesting observable is the analyzing power  $A_y$  for nd elastic scattering with polarized neutrons. Theoretical predictions of standard, high precision NN potentials cannot explain the data for  $A_y$ . The data are underestimated by  $\approx 30\%$  in the region of  $A_y$  maximum which occurs in region of c.m. angles  $\Theta_{cm} \approx 120^\circ$ . Combining standard NN potentials with commonly used models of a 3NF such as TM99 or Urbana IX models removes approximately only half of the discrepancy with respect to the data (see Fig. 1).

When instead of standard forces chiral NN interactions are used, the predictions for  $A_y$  vary with the order of chiral expansion. Theory based on NLO interactions clearly overestimates the  $A_y$  data while N<sup>2</sup>LO forces give quite a good description of them (see Fig. 1) leading thus to disappearance of  $A_y$ -puzzle. Only when N<sup>3</sup>LO NN chiral forces are used, the picture resembles again the one for standard forces, with clear discrepancy between theory and data in the region of  $A_y$  maximum (see Fig. 1 where bands of predictions for five versions of the Bochum NLO, N<sup>2</sup>LO and N<sup>3</sup>LO potentials with cut-off parameters from Table I are shown). Such behaviour can be traced back to a high sensitivity of  $A_y$  to  ${}^3P_j$  NN force components and to the fact, that only at N<sup>3</sup>LO order of chiral expansion the experimental  ${}^3P_j$  phases [22, 23], especially  ${}^3P_2$ - ${}^3F_2$ , are properly reproduced (see also Fig. 2).

The question arises if consistent chiral N<sup>3</sup>LO 3NF's can provide explanation for the low energy  $A_y$ -puzzle. In this first investigation we included all long-range contributions to N<sup>3</sup>LO 3NF with

the exception of  $1/m$  corrections. Additionally, the  $2\pi$ -exchange-contact term was omitted in the short-range part of 3NF. In Fig. 3 we show for the second cut-off parameter from Table I a typical dependence of  $c_E$  and  $c_D$  parameters which reproduce the experimental triton binding energy. The requirement to reproduce in addition also  ${}^2a_{nd}$  scattering length leads to  $c_E$  and  $c_D$  values shown in Table I and  $A_y$  values shown in Fig. 4 by dashed-dotted (blue) line. It turns out that adding that N<sup>3</sup>LO 3NF does not improve the description of  $A_y$ ; on the contrary, even lowers slightly the maximum of  $A_y$  increasing thus a discrepancy between the theory and the data.

In order to check how restrictive is the requirement to reproduce in addition to  ${}^3\text{H}$  binding energy also the experimental value of  ${}^2a_{nd}$  we show in Fig. 4 also a band of predictions for  $(c_E, c_D)$  pairs from Fig. 3. Since that band is narrow it implies that even when allowing for more freedom, that is without reproducing of  ${}^2a_{nd}$ , the  $A_y$ -puzzle cannot be explained by that N<sup>3</sup>LO 3NF.

In Fig. 5 we show bands of predictions for  $A_y$  using N<sup>3</sup>LO chiral NN potentials for five values of cut-off's and combining them with N<sup>3</sup>LO 3NF with  $(c_E, c_D)$  pairs from Table I. It is clear that N<sup>3</sup>LO 3NF without  $1/m$  corrections and  $2\pi$ -contact term is not able to explain the  $A_y$ -puzzle.

The results for the cross section at incoming neutron energy 14.1 MeV shown in the left part of Fig. 4 exemplify negligible 3NF effects for the elastic scattering cross section at low energies.

## B. Breakup

Cross sections for the symmetric-space-star (SST) and quasi-free-scattering (QFS) configurations of the nd breakup are very stable with respect to the underlying dynamics. Different potentials, alone or combined with standard 3N forces, provide practically the same SST and QFS cross sections [29]. Also the chiral N<sup>3</sup>LO 3NF without relativistic  $1/m$  corrections and short-range  $2\pi$ -contact term is no exception and cannot explain the discrepancy between the theory and the data found for the SST configuration [30] (Fig.6). At low energies the cross sections in the SST and QFS configurations are dominated by the S-waves. For the SST configuration the largest contribution to the cross section comes from the  ${}^3S_1$  partial wave, while for neutron-neutron (nn) QFS the  ${}^1S_0$  partial wave dominates. Neglecting rescattering, the QFS configuration resembles free NN scattering. For free, low-energy neutron-proton (np) scattering one expects contributions from  ${}^1S_0$  np and  ${}^3S_1$  force components. For free nn scattering only the  ${}^1S_0$  nn channel is allowed. That implies that nn QFS would be a powerful tool to study the nn interaction. The measurements of np QFS cross sections have shown good agreement of data with theory [31], confirming thus good knowledge of the np force. For nn QFS it was found that theory underestimates the data by  $\approx 20\%$

[31]. The large stability of the QFS cross sections with respect to the underlying dynamics, means that the present day  $^1S_0$  nn interaction is probably incorrect [29, 32, 33].

### III. HIGHER ENERGIES

Studies performed with standard NN potentials revealed that clear discrepancies between theory and data occur for increasing incoming nucleon energy. They start to appear around  $E_N^{lab} \approx 60$  MeV for elastic scattering cross sections and spin observables and their magnitude grows with the energy of a 3N system [10, 13]. Fig.7 and Fig.8 exemplify them for the total nd interaction cross section and elastic scattering angular distributions, respectively. Combining standard NN potentials with commonly used 3NF's such as TM99 or Urbana IX models, leads to a good description of data for cross sections up to  $\approx 130$  MeV (see Fig.7 and Fig.8), fails however completely at higher energies. Also for spin observables at higher energies a complex pattern of angular and energy discrepancies between theory based on standard nuclear forces and data was revealed. That pattern cannot be explained even when standard models of 3NF's are included into calculations [12, 34, 35]. 3N continuum relativistic calculations have shown that relativistic effects, even when 3NF's are included, are negligible for the elastic scattering spin observables and raise the elastic cross section at backward angles [18] only slightly at higher energies. It implies that large discrepancies between theory and data as well as their complex pattern at higher energies are caused by other terms contributing to 3NF, possibly short range 3NF components. With the increasing energy of the 3N system they play a more and more important role. Consistent N<sup>3</sup>LO NN and 3N forces provide thus a unique possibility to check if such a scenario of increasing importance of different 3NF terms is able to provide a good description of observables in 3N reactions at higher energies.

The basic question is if the application of chiral forces to 3N continuum can be justified and extended to energies as high as 200 MeV of incoming nucleon lab. energy? At that energy the value of the expansion parameter  $p/\Lambda \approx 0.45$  therefore application of chiral forces should be possible. However, before taking this step, problems arising from the cut-off dependence of chiral N<sup>3</sup>LO NN force for higher energy predictions should be resolved.

A number of N<sup>3</sup>LO potentials with different cut-off parameter ranging from 414 – 700 MeV (see Table I and II) were developed by the Bochum [21] and Idaho [20] groups, which equally well describe the experimental NN phase-shifts up to  $\approx 200$  MeV with the same high precision as standard NN potentials. However, changing the cut-off in such a wide range of values leads to deuteron wave functions which vary not only between themselves but also with respect to deuteron

wave functions of standard NN potentials at momenta around  $p \approx 2 \text{ fm}^{-1}$  (see Fig.9) or distances around  $r \approx 1.5 \text{ fm}$  (see Fig.10). Since nd elastic scattering transition amplitude Eq. (3) contains an exchange term  $\phi'PG_0^{-1}\phi$  determined by a deuteron wave function, it is necessary to check to what extent the variations of a deuteron wave function with a cut-off parameter are reflected in elastic scattering observables. With increasing energy of the incoming nucleon, the relative nucleon-deuteron momentum  $q_0$  grows, taking value  $q_0 = 2.07 \text{ fm}^{-1}$  at  $E_N^{lab} = 200 \text{ MeV}$ . Exactly at this value of momentum the largest variations of the deuteron wave function for different NN N<sup>3</sup>LO chiral forces occur (see Fig.9).

To study the influence of different cut-offs and corresponding deuteron wave functions on elastic scattering observables we solved the 3N Faddeev equation at three energies: 65 MeV, 135 MeV, and 200 MeV, with the Bochum N<sup>3</sup>LO (five cut-off values of Table I) and N<sup>3</sup>LO Idaho (four cut-off values of Table II) NN potentials. In order to check how results change with the order of the chiral expansion we also performed such calculations with the Bochum N<sup>2</sup>LO (five cut-off values of Table I) NN interactions.

In Figs. 11, 12, and 13 in the left column we show a band of predictions obtained for nd elastic scattering cross section at those three energies and in the right column “cross sections” calculated with the  $\phi'PT\phi$  term (lines peaked at forward angles) and with the exchange term  $\phi'PG_0^{-1}\phi$  (lines peaked at backward angles) separately. At  $E_N^{lab} = 65 \text{ MeV}$  where  $q_0 = 1.18 \text{ fm}^{-1}$  the “exchange term” cross sections start to deviate below  $\Theta_{cm} \approx 80^\circ$ . In this angular region they are more than one order of magnitude smaller than “ $PT$ -term” cross sections. As a consequence a narrow band of predictions for the cross section is obtained for all values of the cut-off parameter in the case of the Bochum and Idaho N<sup>3</sup>LO potentials. At 135 MeV, where  $q_0 = 1.7 \text{ fm}^{-1}$ , the different cut-off values lead to “exchange-term” cross sections of quite different angular dependence. It falls down drastically with decreasing c.m. angle for smaller cut-off values. That behavior is seen even more clearly at 200 MeV, where  $q_0 = 2.07 \text{ fm}^{-1}$ . Since with increasing energy at larger c.m. angles the exchange-term gets more important compared to the  $PT$  term, the resulting band of cross section predictions becomes broader, especially at 200 MeV. At 135 MeV, in spite of the fact that the band is rather narrow, one sees also influence of the deuteron wave function on the cross section, which leads to different angular behavior of the N<sup>3</sup>LO Bochum and Idaho predictions, especially in the region of the cross section minimum.

In Fig.11 we show the predictions of the Bochum N<sup>2</sup>LO potentials. Since N<sup>2</sup>LO deuteron wave functions do not differ significantly and behave similarly to the deuteron wave functions of standard NN forces (see Fig.8) also their influence on the elastic scattering cross sections is negligible. The

growing band width of  $N^2\text{LO}$  predictions reflects the decreasing quality of experimental NN phase-shifts description by  $N^2\text{LO}$  forces with increasing energy. Taking  $N^3\text{LO}$  forces reduces that width significantly (see Figs. 12 and 13).

One could argue that such behavior restricts the application of  $\chi\text{PT}$  forces to a rather narrow range of 3N system energies below  $\approx 100$  MeV of the incoming nucleon lab. energy. If that was true, it would make the application of the chiral approach impossible in the most interesting region of energies, where the consistency between 2N- and 3N-forces plays the most important role. One possible way to resolve this problem would be to restrict the range of cut-off to larger values. The other is connected to the omission of 3NF's in above 3N continuum calculations. Since neglecting a 3NF in nuclear Hamiltonian is an artifact and one should use both NN and 3NF's simultaneously, one could argue that when both are applied the dependence on the cut-off parameter would be diminished. To check if that is the case one must perform fully converged calculations with 2N and 3N chiral forces included. At higher energies much more partial waves are required. The large number of terms contributing to the chiral  $N^3\text{LO}$  3NF and huge computer resources needed to calculate their matrix elements in higher partial waves preclude presently fully converged nd calculations at higher energies. Therefore an approach in which partial wave decomposition is avoided and instead vector Jacobi momenta are used is desirable. In the following section we review the present state of such three-dimensional approach to 3N Faddeev equations.

#### IV. THREE-DIMENSIONAL FORMULATIONS

We restrict ourselves to the momentum space integral equation formulations.

As already stated, below the pion production threshold the momentum space Faddeev equations for three-nucleon (3N) scattering can be solved with high accuracy for essentially all modern two- and three-nucleon forces. In these calculations angular momentum eigenstates for the two- and three-body systems are used. This partial wave decomposition (PWD) replaces continuous angular variables by a finite set of orbital angular momentum quantum numbers and allows one to reduce the number of continuous variables to only two.

For low projectile energies the procedure of employing orbital angular momentum components is well justified. Physics arguments are related to the centrifugal barrier and the short range of the nuclear force. Besides, in a numerical realization, a fast convergence of the observables with respect to the number of partial wave states is easily achieved.

However, when considering 3N scattering at higher energies, a much larger number of partial

wave states is required before results become fully convergent. This has obvious consequences for the computational resources required in the calculations. A considerable effort is required, especially when 3N forces with numerous spin-momentum and isospin structures are implemented. Preparation of their matrix elements in the partial wave representation, either analytically or numerically, is highly nontrivial when the set of partial waves grows rapidly. Thus it appears natural to avoid PWD and work directly with vector variables. We describe below the remarkable progress made in this field.

The main problem in 3N scattering is related to a treatment of the singularity in the free 3N propagator above the break-up threshold. The way to deal with this difficulty was introduced in [43], where subtraction techniques were employed to integrate the logarithmic singularities. For quite a long time this approach seemed to be the only possibility and just minor deviations from the scheme of [43] were introduced. For example, in [44] the logarithmic singularities were integrated quasi-analytically using splines. Only very recently, a new form of the integral kernel for 3N scattering was found, first in the context of the partial wave decomposed Faddeev equation [45] and later for its three dimensional (3D) realization in the case of three bosons [46]. In this new approach the treatment of the 3N Faddeev equation becomes essentially as simple as the treatment of the two-body Lippmann-Schwinger equation.

Without that new insight, it was most natural in the past to proceed also for the 3D treatments of the 3N Faddeev equation in the following way. First, the calculation of the deuteron wave function and the two-nucleon (2N) scattering t-matrices was required to provide an input to this equation. Then, typically the Faddeev equation for the 3N bound state was solved. In this case the 3N energy is negative, so one encountered no problems with the 3N propagator. The other ingredients of the formalism could be, however, carefully tested. In particular, the permutation operator and the t-matrices for negative 2N energies had to be well mastered in the bound state calculations. Finally, the full problem of nucleon-deuteron (Nd) scattering above the break-up threshold without or with a 3N force could be studied. In this case not only the number of variables was bigger due to the presence of the external momentum, but also the singularity of the free 3N propagator had to be taken into account.

If one is interested not only in pure  $Nd$  scattering but also in reactions involving 3N scattering states, like in the description of inelastic electron scattering on  ${}^3\text{H}$ ,  $e + {}^3\text{H} \rightarrow e' + n + d$ , then it is of great importance that the ingredients of the 3D formalism: the deuteron and  ${}^3\text{H}$  wave functions as well as the neutron-deuteron scattering state are prepared consistently.

### A. Nucleon-nucleon scattering in three dimensions

Nucleon-nucleon scattering was treated without PWD already more than twenty years ago. In [47, 48] the time-dependent Schrödinger equation was solved eventually for a one-boson exchange potential. It is worth mentioning that in the latter paper the general form of the potential between two spin-1/2 particles was used to simplify the calculations.

Later in [49] quasielastic electron scattering was investigated and the final-state interaction was taken into account by evaluating the two-body t-matrix directly in 3D for the Malfliet-Tjon (MT III) local spin independent force [50]. More systematically the angular and momentum dependence of the t-matrix was studied in the same 3D approach on as well as off the energy shell in [51], both for positive and negative  $2N$  energies. In this very informative paper the behaviour of the t-matrix in the vicinity of bound-state pole and resonance poles in the second energy sheet were also investigated for different Malfliet-Tjon-type potentials.

Another alternative to the usual PWD technique was outlined in [52]. There the two-body Lippmann-Schwinger equation was written in a numerically solvable form using helicity theory and taking advantage of the symmetries of the NN interaction. The numerical examples were based on the Bonn OBEPR potential [53]. The helicity formalism was also used in [54] (with slightly modified final equations) for two quite different NN potentials, the Bonn B [55] and the Argonne V18 [3]. The same helicity approach was subsequently used by S. Bayegan *et al.* [56] in 3D calculations of NN bound and scattering states with a chiral N<sup>3</sup>LO potential [21]. In all these works an excellent agreement with the results based on standard PWD was reported.

Inclusion of the Coulomb interaction on top of a local spin-dependent short-range interaction in two-body scattering was carried out in [57]. The calculations are not performed for the NN system but their implications are important for all results, where the screening and renormalization approach is used to treat the Coulomb interaction.

Parallel to the above mentioned nonrelativistic studies, 3D formulations of the scattering equations were studied also for the relativistic equations. In [58] this was outlined in the case of pion-nucleon and NN scattering treated via the Bethe-Salpeter equation. In [59] a numerical method, based on the Padé summation, was introduced to solve the covariant spectator equation without partial wave decomposition, and applied to the NN system.

Last but not least we would like to mention calculations of the NN t-matrix, which employ directly momentum vectors and use spin-momentum operators multiplied by scalar functions of the momentum vectors. This approach stems from the fact that a general NN force being invariant

under time-reversal, parity, and Galileo transformations can depend only on six linearly independent spin-momentum operators. The representation of the NN potential using spin-momentum operators leads to a system of six coupled equations of scalar functions (depending on momentum vectors) for the NN t-matrix, once the spin-momentum operators are analytically calculated by performing suitable trace operations. This treatment, formulated in [60], can be considered as a natural extension for two spin-1/2 particles of the calculations described in [51]. In [60] numerical examples for the Bonn B [55] and chiral N2LO potentials [21, 61, 62] were presented. Later in [63] the same approach (with a modified choice of the basis spin-momentum operators) was applied to the Argonne V18 potential [3]. Further variations of this method and inclusion of the Coulomb force can be found in [64, 65]. Finally, the application of this operator based approach to the deuteron electro-disintegration process was discussed in [66].

## B. Few-nucleon bound states in three dimensions

We start with the deuteron representations formulated without any resort to PWD.

In [67] the helicity representation developed previously for NN scattering [54] was applied to the 2N bound state and the deuteron eigenvalue equation in the helicity basis was solved with the Bonn B potential [55]. In the same paper the deuteron wave function in the so-called (momentum space) operator form was also derived. In this representation the whole information about the deuteron is given by two scalar functions,  $\phi_1(p)$  and  $\phi_2(p)$ , which are closely related to the standard  $S$  and  $D$  components of the deuteron. The direct set of two coupled equations for  $\phi_1(p)$  and  $\phi_2(p)$  was derived only later in [68]. That derivation included simple trace operations, which helped eliminate spin degrees of freedom and led to analytically given sets of scalar functions depending on momentum vectors only. Numerical examples for the Bonn B [55] and chiral N2LO potentials [21, 61, 62] were published in [60]. Corresponding three dimensional calculations of 2N binding energies with chiral N3LO potentials [21] performed in the helicity formalism were reported in [56].

As already mentioned, the work on NN scattering has very often a preparatory character and further application of the t-matrices are usually planned. This is true also in the case of the 3D calculations. Results of [51] were later used in [69] three-body bound-state calculations without PWD with Malfliet-Tjon-type NN potentials, neglecting spin and isospin degrees of freedom. In the subsequent paper [70] the scheme from [69] was extended to include scalar two-meson exchange three-body forces.

The Teheran group published several papers dealing with 3D solutions of the 3N and even

four-nucleon (4N) bound states [71–78]. They started with a formulation, which neglected the spin-isospin degrees of freedom [71] and introduced step by step improved dynamical ingredients to their framework, performing calculations with more realistic NN potentials (like the Bonn B one in [72, 73]) and including additionally a 3N force (for example the Tucson-Melbourne 3N potential in [75]). The 3D t-matrices - an input to the systems of coupled equations - were obtained with the helicity representation of [54].

Finally, we list publications dealing with the 3D treatment of the 3N bound state which relies on the general form of the 2N t-matrix and the operator form of the 3N bound state introduced in [79]. The latter consists of eight operators built from scalar products of relative momentum and spin vectors, which are applied to a pure 3N spin 1/2 state. Each of the operators is multiplied by a scalar function of the relative momentum vectors. In [68] one Faddeev equation for identical bosons was replaced by a finite set of coupled equations for scalar functions which depend only on three variables. The inclusion of a 3N force into this 3D Faddeev framework was also discussed. Further elements of this formalism, for example the construction of the full wave function from the Faddeev amplitude, and first numerical results for chiral 2N and 3N N<sup>2</sup>LO nuclear forces were provided in [80].

### C. Nucleon-deuteron scattering in three dimensions

Here we come to the essential, from the point of view of the present paper, 3D calculations of  $Nd$  scattering.

They were initiated in [81], soon after the t-matrix [51] and the three-body bound state [69] were successfully treated without employing of PWD. Although in [81] the authors focused on scattering below the three-body breakup threshold and avoided the singularity of the free three-body propagator, they had to tackle the pole in the two-body t-matrix at the energy corresponding to the two-body bound state. Spin and isospin degrees of freedom were neglected in that pioneering paper. This framework was naturally extended to higher energies in [44], where the Faddeev equation was solved for the three-boson case using the Padé method. The elastic differential cross section, semiexclusive  $d(N, N')$  cross sections, and the total cross sections for the elastic and breakup processes at energies up to about 1 GeV were calculated.

At such high projectile energies special relativity is expected to become relevant. The key advantage of a formulation of the Faddeev equations in terms of vector variables lies in the fact that using them, the relativistic three-body problem can be formulated more easily than in PWD scheme.

To achieve this goal, in [82] authors worked within the framework of Poincaré invariant quantum mechanics, where the dynamical equations have the same number of variables as the corresponding nonrelativistic equations. The equations used to describe the relativistic few-body problem have even the same operator form as the nonrelativistic ones but their ingredients are different. This was discussed in detail in [82] and the authors restricted themselves to the leading-order term of the Faddeev multiple scattering series within the framework of Poincaré invariant quantum mechanics, since it already contained many relativistic ingredients. In that paper kinematical and dynamical relativistic effects on selected observables were systematically studied. As later found in [46, 83–85], the truncation of the multiple scattering series to the first term was not always justified. This insight became possible, when the full solution to the relativistic Faddeev equation for three bosons had been obtained. Only then convergence of the multiple scattering series could be investigated as a function of the projectile energy in different scattering observables and configurations. Based on a Malfliet-Tjon interaction, which generated the same nonrelativistic and relativistic observables in the 2N system, observables for elastic and breakup scattering were calculated and compared to non-relativistic ones. That gave first insight to “relativistic effects” in  $Nd$  scattering. It is also worth noticing that the cross sections calculated in [86] at 500 MeV are in quite good agreement with experimental data, in spite of the simple nature of the model interaction. One may hope that in the future a similar framework will be built based on realistic NN forces.

A completely different path was chosen in [87]. There only the first term of the multiple scattering series generated by the Faddeev equations was considered but authors used realistic NN forces, the Bonn B [55] and the Argonne V18 [3] potentials. Including spin degrees of freedom, it was possible to calculate some polarization observables for the  $d(p, n)pp$  reaction and compare them with the results of PWD calculations. The NN t-matrix elements were calculated in the helicity representation defined in [54]. Based on the information available from calculations using PWD, this framework has to be extended towards full solution of the Faddeev equation. Also 3N forces have to be included in this scheme.

We are not aware of a regular paper from the Teheran group about their treatment of  $Nd$  scattering in 3D, although photodisintegration of  ${}^3\text{H}$  based on realistic NN interactions with full inclusion of final state interactions among the outgoing nucleons reported in [88], requires the same technical achievements as  $Nd$  scattering.

From our point of view, a very promising way to proceed towards (at least) nonrelativistic 3D treatment of  $Nd$  scattering was formulated in [89]. The recently developed “operator” formalism for two- and three-nucleon bound states in three dimensions [60, 68, 80] was extended to the realm

of nucleon-deuteron scattering. The aim was here to formulate the momentum space Faddeev equations in such a fashion that the final equations would be reduced to spin-independent scalar functions in the same spirit as already worked out for the 2N and 3N bound states. The numerical realization of this framework is in progress.

## V. SUMMARY AND OUTLOOK

Recent derivation of the N<sup>3</sup>LO 3NF opened the possibility to test consistent two- and three-nucleon chiral forces at that order in few-nucleon applications. Since with the growing order of the chiral expansion the number of terms contributing to the chiral 3NF increases significantly, a prerequisite to such applications was a development of fast and efficient method of automated partial wave decomposition. Using that method we applied for the first time chiral N<sup>3</sup>LO 3NF (still without the short-range  $2\pi$ -contact term and  $1/m$  relativistic corrections) to low energy nd elastic scattering and breakup. It turns out that N<sup>3</sup>LO 3NF cannot explain the low-energy  $A_y$ -puzzle. That result indicates possible drawbacks of low-energy  ${}^3P_j$  NN phase-shifts or/and on the lack of some spin-isospin-momenta structures in N<sup>3</sup>LO 3NF. The standard chiral perturbation theory formulation based on pions and nucleons as the only explicit degrees of freedom still misses at N<sup>3</sup>LO some physics associated with intermediate  $\Delta$  excitations, which can be to some extent accounted for only at N<sup>4</sup>LO order [36, 37]. Since  $\Delta$  provides an important mechanism leading to a new form of 3NF, in the next step one should apply that recently derived N<sup>4</sup>LO 3NF [36, 37] in calculations of nd reactions.

Higher-energy nd reactions, in which clear evidence for large 3NF effects was found, call for a three-dimensional treatment of the 3N Faddeev equations. The rather simple form of 2- and 3-nucleon chiral forces, when expressed in terms of Jacobi momentum vectors, encourages approaches which altogether avoid partial wave decomposition. Studies of the cut-off dependence of N<sup>3</sup>LO NN chiral interaction in higher-energy nd elastic scattering revealed preference for larger cut-off values. The use of lower cut-offs would preclude applications of N<sup>3</sup>LO chiral dynamics in that interesting region of energies.

### Acknowledgments

The authors would like to thank Prof. E. Epelbaum for very constructive and valuable discussions. This work was supported by the Polish National Science Center under Grant No. DEC-

2011/01/B/ST2/00578. It was also partially supported by the Japan Society for Promotion of Science (JSPS ID No. S-12028), and by the European Community-Research Infrastructure Integrating Activity “Exciting Physics Of Strong Interactions” (acronym WP4 EPOS) under the Seventh Framework Programme of EU. The numerical calculations have been performed on the supercomputer cluster of the JSC, Jülich, Germany and Ohio Supercomputer Centre, USA (Project PAS0680). We acknowledge support by the Foundation for Polish Science - MPD program, co-financed by the European Union within the Regional Development Fund.

- 
- [1] W. Glöckle, H. Witała, D. Hüber, H. Kamada, J. Golak, Phys. Rep. **274**, 107-285 (1996).
- [2] D. Hüber, H. Kamada, H. Witała, and W. Glöckle, Acta Physica Polonica **B28**, 1677-1685 (1997).
- [3] R.B. Wiringa, V.G.J. Stoks, R. Schiavilla, Phys. Rev. **C51**, 38-51 (1995).
- [4] R. Machleidt, F. Sammarruca, and Y. Song, Phys. Rev. **C53**, R1483-R1487 (1996).
- [5] V.G.J. Stoks, R.A.M. Klomp, C.P.F. Terheggen, J.J. de Swart, Phys. Rev. **C49**, 2950-2962 (1994).
- [6] S.A. Coon and H.K. Han, Few Body Syst. **30**, 131-141 (2001).
- [7] B.S. Pudliner, V.R. Pandharipande, J. Carlson, S.C. Pieper, R.B. Wiringa, Phys. Rev. **C56**, 1720-1750 (1997).
- [8] J.L. Friar, G.L. Payne, V.G.J. Stoks, J.J. de Swart, Phys. Lett. **B311**, 4-8 (1993).
- [9] A. Nogga, D. Hüber, H. Kamada, and W. Glöckle, Phys. Lett. **B409**, 19-25 (1997).
- [10] H. Witała, W. Glöckle, J. Golak, A. Nogga, H. Kamada, R. Skibiński, and J. Kuroś-Żołnierczuk, Phys. Rev. **C63**, 024007-024018 (2001).
- [11] H. Witała, W. Glöckle, D. Hüber, J. Golak, and H. Kamada, Phys. Rev. Lett. **81**, 1183-1186 (1998).
- [12] K. Sekiguchi et al., Phys. Rev. **C65**, 034003-034018 (2002).
- [13] W.P. Abfalterer et al., Phys. Rev. Lett. **81**, 57-60 (1998).
- [14] H. Witała, H. Kamada, A. Nogga, and W. Glöckle, Phys. Rev. **C59**, 3035-3046 (1999).
- [15] H. Witała, J. Golak, W. Glöckle, H. Kamada, Phys. Rev. **C71**, 054001-054012 (2005).
- [16] H. Witała, J. Golak, R. Skibiński, W. Glöckle, W.N. Polyzou, H. Kamada, Phys. Rev. **C77**, 034004-034016 (2008).
- [17] H. Kamada, W. Glöckle, Phys. Lett. **B 655**, 119-125 (2007).
- [18] H. Witała, J. Golak, R. Skibiński, W. Glöckle, H. Kamada, and W.N. Polyzou, Phys. Rev. **C83**, 044001-044020 (2011).
- [19] E. Epelbaum, A. Nogga, W. Glöckle, H. Kamada, U.-G. Meißner, and H. Witała, Phys. Rev. **C 66**, 064001-064017 (2002).
- [20] D.R. Entem and R. Machleidt, Phys. Rev. **C68**, 041001(R)-041005(R) (2003).
- [21] E. Epelbaum, W. Glöckle, and U.-G. Meißner, Nucl. Phys. **A747**, 362-424 (2005).
- [22] J. R. Bergervoet, P.C. van Campen, R.A.M. Klomp, J.-L. de Kok, T.A. Rijken, V.G.J. Stoks, and J.J. de Swart, Phys. Rev. **C41**, 1435-1452 (1990).
- [23] V.G.J. Stoks, R.A.M. Klomp, M.C.M. Rentmeester, and J.J. de Swart, Phys. Rev. **C48**, 792-815 (1993).
- [24] V. Bernard, E. Epelbaum, H. Krebs, and U.-G. Meißner, Phys. Rev. **C 77**, 064004-064016 (2008).
- [25] V. Bernard, E. Epelbaum, H. Krebs, and U.-G. Meißner, Phys. Rev. **C84**, 054001-054012 (2011).
- [26] J. Golak, D. Rospędzik, R. Skibiński, K. Topolnicki, H. Witała, W. Glöckle, A. Nogga, E. Epelbaum, H. Kamada, Ch. Elster, Eur. Phys. J. **A43**, 241-250 (2010).
- [27] R. Skibiński, J. Golak, K. Topolnicki, H. Witała, H. Kamada, W. Glöckle, A. Nogga, Eur. Phys. J. **A47** 48-63 (2011).

- [28] H. Witała, A. Nogga, H. Kamada, W. Glöckle, J. Golak, R. Skibiński, Phys. Rev. **C68**, 034002-034009 (2003).
- [29] H. Witała and W. Glöckle, J. Phys. G: Nucl. Part. Phys. **37**, 064003-13 (2010).
- [30] H. R. Setze et al., Phys. Lett. **B388**, 229-234 (1996).
- [31] A. Siepe, J. Deng, V. Huhn, L. Wätzold, Ch. Weber, W. von Witsch, H. Witała, W. Glöckle, Phys. Rev. **C65**, 034010–34016 (2002).
- [32] H. Witała and W. Glöckle, Phys. Rev. **C83**, 034004-034011 (2011).
- [33] H. Witała and W. Glöckle, Phys. Rev. **C85**, 064003-064011 (2012).
- [34] K. Sekiguchi et al., Phys. Rev. **C70**, 014001-014017 (2004).
- [35] K. Hatanaka et al., Phys. Rev. **C66**, 044002-044011 (2002).
- [36] H. Krebs, A. Gasparyan, and E. Epelbaum, Phys. Rev. **C85**, 054006-054020 (2012).
- [37] H. Krebs, A. Gasparyan, and E. Epelbaum, Phys. Rev. **C87**, 054007-054032 (2013).
- [38] W. Tornow et al., Phys. Lett. **B257**, 273-277 (1991).
- [39] W. Tornow, C.R. Howell, R.C. Byrd, R.S. Pedroni, and R.L. Walter, Phys. Rev. Lett. **49**, 312-315 (1982).
- [40] W. Tornow, R.C. Byrd, C.R. Howell, R.S. Pedroni, and R.L. Walter, Phys. Rev. **C27**, 2439-2442 (1983).
- [41] A. C. Berick, R. A. J. Ridle, and C. M. York, Phys. Rev. **174**, 1105-1111 (1968).
- [42] Y. Maeda et al., Phys. Rev. **C76**, 014004-014016 (2007).
- [43] H. Witała, W. Glöckle, Th. Cornelius, Phys. Rev. **C39**, 384-390 (1989).
- [44] H. Liu, Ch. Elster, and W. Glöckle, Phys. Rev. **C72**, 054003-054019 (2005).
- [45] H. Witała, W. Glöckle, Eur. Phys. J. **A37**, 87-95 (2008).
- [46] Ch. Elster, W. Glöckle, H. Witała, Few-Body Syst. **45**, 1-10 (2009).
- [47] J. Holz and W. Glöckle, J. Comp. Phys. **76**, 131-158 (1988).
- [48] J. Holz and W. Glöckle, Phys. Rev. **C37**, 1386-1402 (1988).
- [49] D. Hüber, W. Glöckle, and A. Bömelburg, Phys. Rev. **C42**, 2342-2357 (1990).
- [50] A. Malfliet and J. A. Tjon, Nucl. Phys. **A127**, 161-168 (1969).
- [51] Ch. Elster, J. H. Thomas, and W. Glöckle, Few-Body Syst. **24**, 55-79 (1998).
- [52] R. A. Rice, Y. E. Kim, Few-Body Syst. **14**, 127-148 (1993).
- [53] R. Machleidt, K. Holinde, Ch. Elster, Phys. Rep. **149**, 1-89 (1987).
- [54] I. Fachruddin, Ch. Elster, and W. Glöckle, Phys. Rev. **C62**, 044002-044020 (2000).
- [55] R. Machleidt, Adv. Nucl. Phys. **19**, 189-376 (1989).
- [56] S. Bayegan, M. A. Shalchi, and M. R. Hadizadeh, Phys. Rev. **C79**, 057001-057004 (2009).
- [57] M. Rodríguez-Gallardo, A. Deltuva, E. Cravo, R. Crespo, and A. C. Fonseca, Phys. Rev. **C78**, 034602-034609 (2008).
- [58] G. L. Caia, V. Pascalutsa, and L. E. Wright, Phys. Rev. **C69**, 034003-034010 (2004).
- [59] G. Ramalho, A. Arriaga, M. T. Peña, Few-Body Syst. **39**, 123-157 (2006).
- [60] J. Golak, W. Glöckle, R. Skibiński, H. Witała, D. Rozpędzik, K. Topolnicki, I. Fachruddin, Ch. Elster,

- and A. Nogga, Phys. Rev. **C81**, 034006-034023 (2010).
- [61] E. Epelbaum, Prog. Part. Nucl. Phys. **57**, 654-741 (2006).
  - [62] E. Epelbaum, H. W. Hammer, and Ulf-G. Meißner, Rev. Mod. Phys. **81**, 1773-1825 (2009).
  - [63] S. Veerasamy, Ch. Elster, W. N. Polyzou, Few-Body Syst., DOI 10.1007/s00601-012-0476-1.
  - [64] R. Skibiński, J. Golak, D. Rozpędzik, K. Topolnicki, H. Witała, Few-Body Syst. **50**, 279-281 (2011).
  - [65] J. Golak, R. Skibiński, H. Witała, K. Topolnicki, W. Glöckle, A. Nogga, H. Kamada, Few-Body Syst. **53**, 237-252 (2012).
  - [66] K. Topolnicki, J. Golak, R. Skibiński, A. E. Elmeshneb, W. Glöckle, A. Nogga, H. Kamada, Few-Body Syst., DOI 10.1007/s00601-012-0479-y.
  - [67] I. Fachruddin, Ch. Elster, and W. Glöckle, Phys. Rev. **C63**, 054003-054016 (2001).
  - [68] W. Glöckle, Ch. Elster, J. Golak, R. Skibiński, H. Witała, H. Kamada, Few-Body Syst. **47**, 25-38 (2010).
  - [69] Ch. Elster, W. Schadow, A. Nogga, and W. Glöckle, Few-Body Syst. **27**, 83-105 (1999).
  - [70] H. Liu, Ch. Elster, W. Glöckle, Few-Body Syst. **33**, 241-258 (2003).
  - [71] M. R. Hadizadeh and S. Bayegan, Proceedings of the 3rd Asia- Pacific Conference, Nakhon Ratchasima, Thailand, July 2005 (World Scientific, Singapore, 2007), p. 16.
  - [72] S. Bayegan, M. R. Hadizadeh, and M. Harzchi, Phys. Rev. **C77**, 064005-064014 (2008).
  - [73] S. Bayegan, M. R. Hadizadeh, M. Harzchi, Few-Body Syst. **44**, 65-67 (2008).
  - [74] M. R. Hadizadeh, L. Tomio, S. Bayegan, AIP Conf. Proc. **1265**, 84 (2010).
  - [75] M. R. Hadizadeh and S. Bayegan, Few-Body Syst. **40**, 171-191 (2007).
  - [76] M. R. Hadizadeh, Lauro Tomio, and S. Bayegan, Phys. Rev. **C83**, 054004-054010 (2011).
  - [77] M. R. Hadizadeh, S. Bayegan, Eur. Phys. J. **A36**, 201-209 (2008).
  - [78] S. Bayegan, M. R. Hadizadeh, W. Glöckle, Prog. Theor. Phys. **120**, 887-916 (2008).
  - [79] I. Fachruddin, W. Glöckle, Ch. Elster, and A. Nogga, Phys. Rev. **C69**, 064002-064017 (2004).
  - [80] J. Golak, K. Topolnicki, R. Skibiński, W. Glöckle, H. Kamada, A. Nogga, Few-Body Syst, DOI 10.1007/s00601-012-0472-5.
  - [81] W. Schadow, Ch. Elster, and W. Glöckle, Few-Body Syst. **28**, 15-34 (2000).
  - [82] T. Lin, Ch. Elster, W. N. Polyzou, and W. Glöckle, Phys. Rev. **C76**, 014010-014032 (2007).
  - [83] T. Lin, Ch. Elster, W. N. Polyzou, H. Witała, and W. Glöckle, Phys. Rev. **C78**, 024002-024020 (2008).
  - [84] W. N. Polyzou, T. Lin, Ch. Elster, W. Glöckle, Few-Body Syst. **44**, 287-289 (2008).
  - [85] Ch. Elster, T. Lin, W. N. Polyzou, W. Glöckle, Few-Body Syst. **45**, 157-160 (2009).
  - [86] T. Lin, Ch. Elster, W.N. Polyzou, W. Glöckle, Physics Letters **B660**, 345-349 (2008).
  - [87] I. Fachruddin, Ch. Elster, and W. Glöckle, Phys. Rev. **C68**, 054003-054021 (2003).
  - [88] S. Bayegan, M. A. Shalchi, M. R. Hadizadeh, EPJ Web Conf. **3**, 04008 (2010).
  - [89] W. Glöckle, I. Fachruddin, Ch. Elster, J. Golak, R. Skibiński, H. Witała, Eur. Phys. J. **A43**, 339-350 (2010).

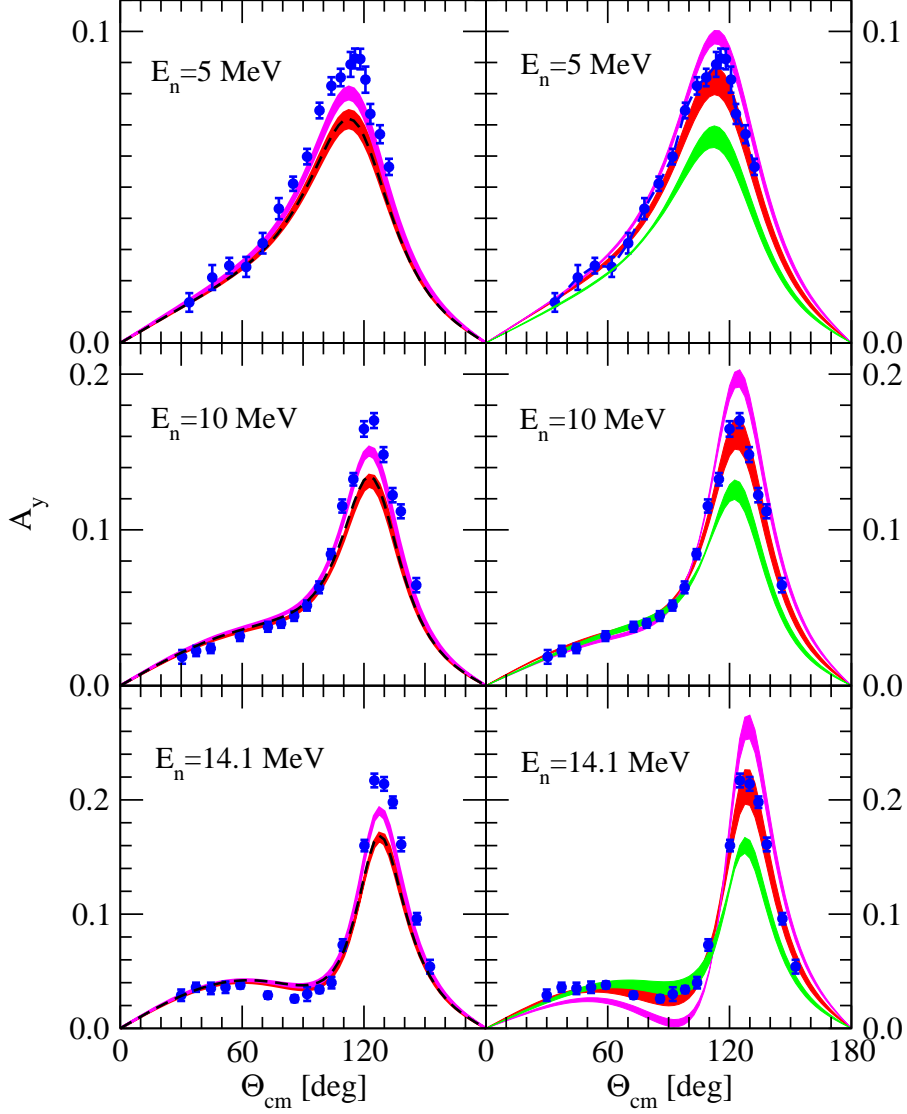


FIG. 1: (color online) The neutron analyzing power  $A_y$  in elastic nd scattering. In the left column the dark shaded (red) and light shaded (magenta) bands show predictions of realistic NN potentials (AV18, CD Bonn, Nijm1 and Nijm2) alone or combined with the TM99 3NF, respectively. The dashed (black) line shows prediction of AV18 + Urbana IX combination. In the right column the magenta (upper), red (middle) and green (low) bands show predictions of the Bochum NLO,  $N^2$ LO, and  $N^3$ LO chiral NN potentials, respectively, for the five cut-off parameters from Table I. The nd data (full blue circles) at 5 MeV are from [38], at 10 MeV from [39], and at 14.1 MeV from [40].

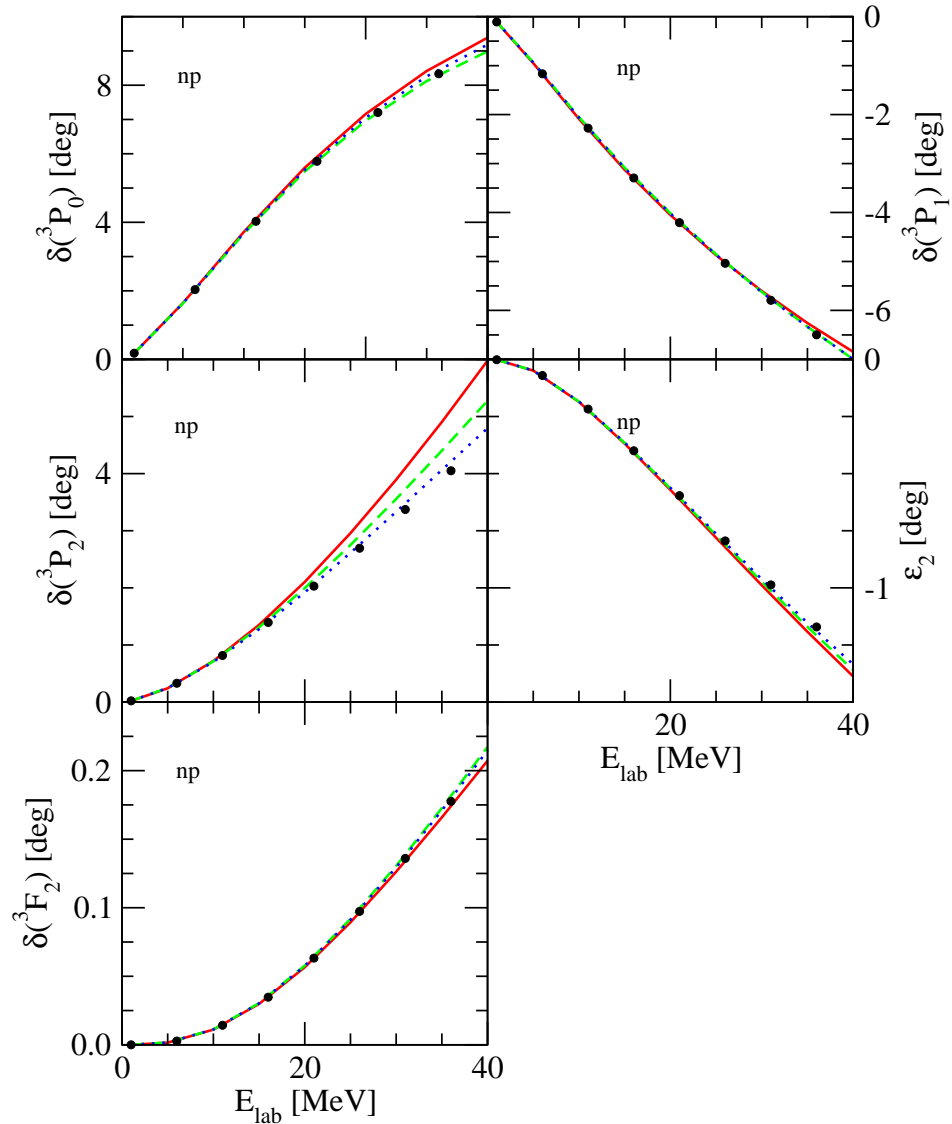


FIG. 2: (color online) The neutron-proton  ${}^3P_j$  phase-shifts as a function of lab. energy  $E_{lab}$ . The solid (red), dashed (green), and dotted (blue) lines show predictions of the Bochum NLO, N<sup>2</sup>LO, and N<sup>3</sup>LO NN potentials with a second cut-off parameter of Table I, respectively. The solid (black) circles are experimental Nijmegen phase-shifts [22, 23].

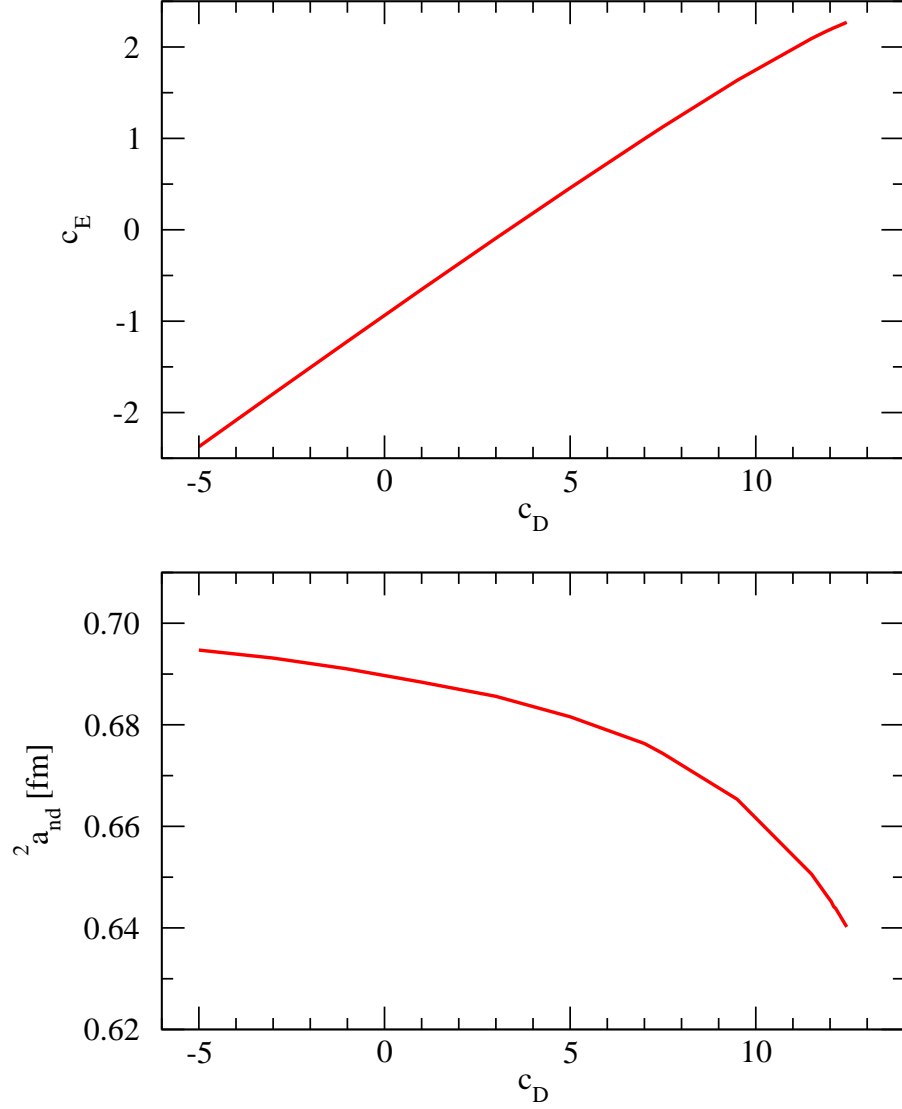


FIG. 3: (color online) Values of  $(c_D, c_E)$  pairs which reproduce  ${}^3\text{H}$  experimental binding energy (upper part) and dependence of the doublet nd scattering length  ${}^2a_{nd}$  on  $c_D$ . The Bochum  $\text{N}^3\text{LO}$  chiral 2N- and 3N-forces were used in calculations with a second cut-off parameter from Table I.

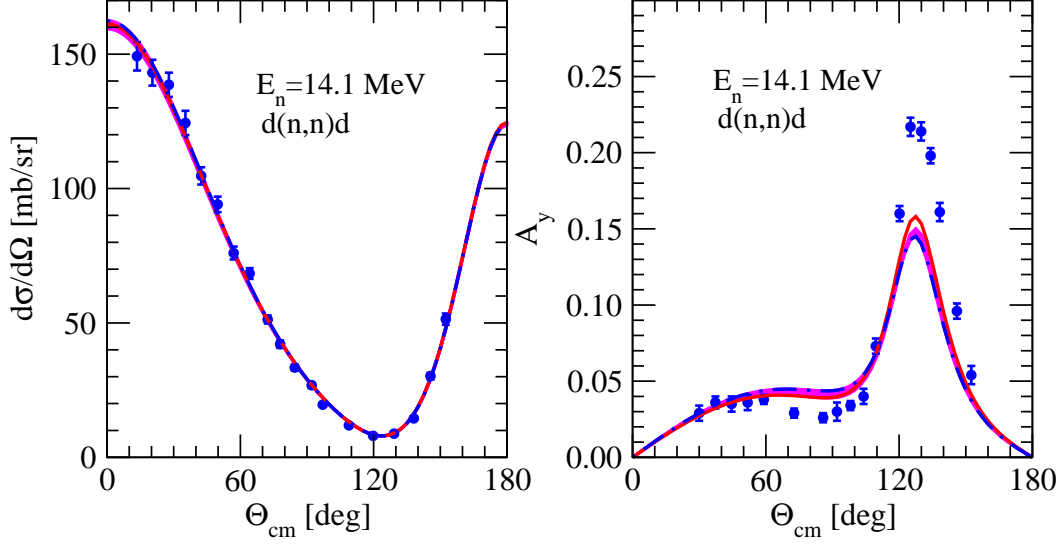


FIG. 4: (color online) The neutron cross section (left part) and analyzing power  $A_y$  (right part) for elastic nd scattering at  $E_n = 14.1$  MeV. The solid (red) line shows predictions of the Bochum  $N^3LO$  NN potential (with the second cut-off parameter from Table I) alone and the dashed-dotted (blue) line results when that potential is combined with the  $N^3LO$  3NF without  $1/m$  corrections and  $2\pi$ -exchange-contact term. The light shaded (magenta) bands show predictions for that combination of NN + 3NF forces with values of  $c_D$  and  $c_E$  parameters from upper part of Fig. 3. The nd data (full blue circles) for the cross section are from [41] and for  $A_y$  from [40].

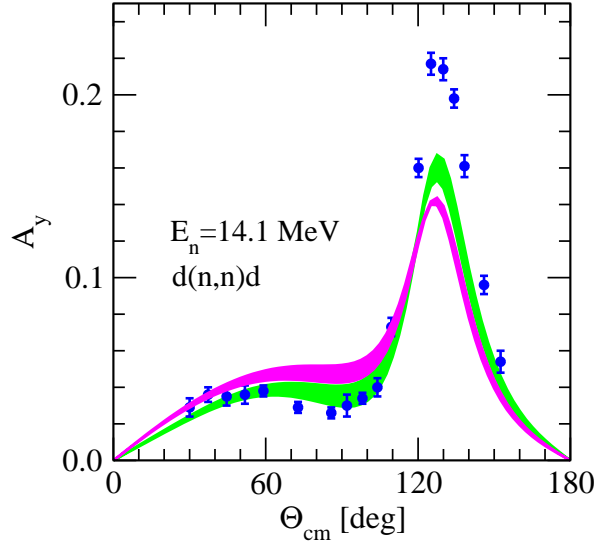


FIG. 5: (color online) The neutron analyzing power  $A_y$  elastic nd scattering at  $E_n = 14.1$  MeV. The light shaded (green) and dark shaded (magenta) bands contain predictions of the Bochum  $N^3LO$  NN potentials with five cut-off parameters of Table I alone and when they are combined with  $N^3LO$  3NF without  $2\pi$ -exchange-contact term, respectively. The nd data (full circles) are from [40].

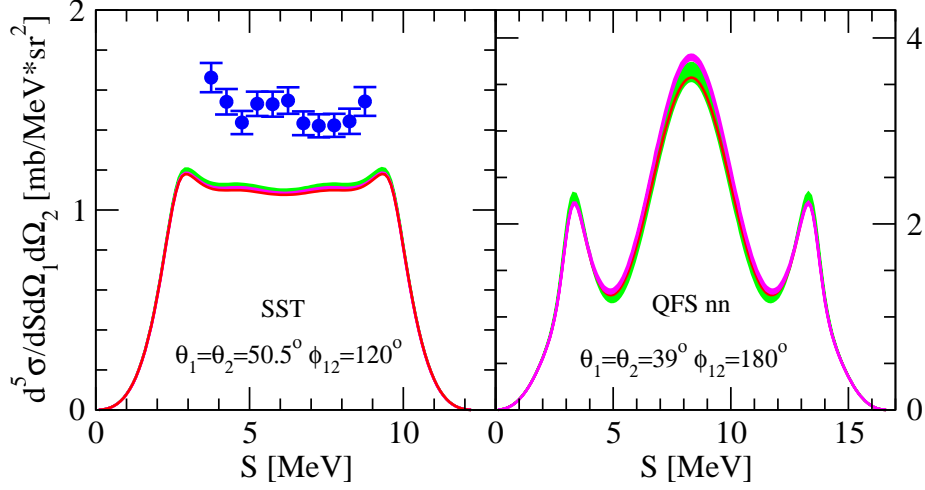


FIG. 6: (color online) The cross section  $d^5\sigma/d\Omega_1 d\Omega_2 dS$  for the  $d(n,nn)p$  breakup reaction as a function of the arc-length  $S$  at  $E_n^{lab} = 13$  MeV for the SST and QFS nn configurations. The light shaded (green) and dark shaded (magenta) bands show predictions of the Bochum  $N^3LO$  NN potentials alone and combined with the  $N^3LO$  3NF (without short-range  $2\pi$ -exchange-contact term) for five different cut-offs of Table I, respectively. The solid (red) line is a prediction obtained with the CD Bonn potential. The full (blue) circles are nd data for the SST configuration from [30].

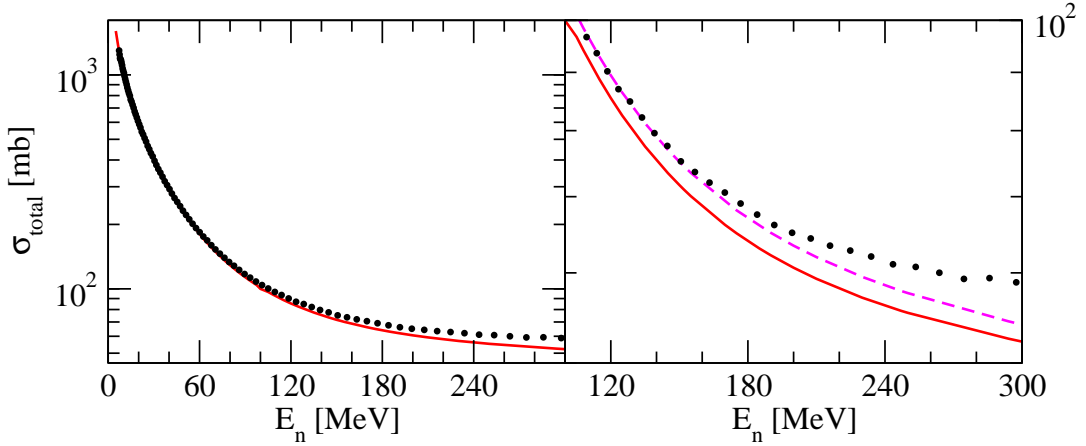


FIG. 7: (color online) The total nd cross section as a function of the neutron lab. energy  $E_n$ . The solid (red) and dashed (magenta) lines show predictions of the CD Bonn potential alone and combined with TM99 3NF, respectively. The black dots are nd data from [13].

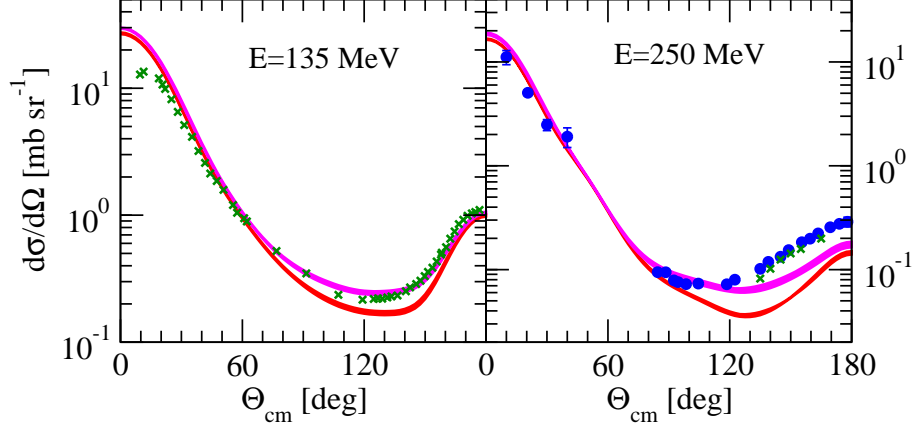


FIG. 8: (color online) The nd elastic scattering angular distributions at 135 MeV and 250 MeV of incoming neutron lab. energy. The dark shaded (red) and the light shaded (magenta) bands are predictions of standard NN potentials (AV18, CD Bonn, Nijm I and II) alone and when they are combined with the TM99 3NF, respectively. The (green) x-es are pd data at 135 MeV from [12] and at 250 MeV from [35]. Full (blue) circles are nd data from [42].

cut-off	$(\Lambda, \tilde{\Lambda})$ [MeV]	$c_D$	$c_E$
1	(450,500)	10.78	-0.172
2	(600,500)	12.00	1.254
3	(550,600)	11.67	2.120
4	(450,700)	7.21	-0.748
5	(600,700)	14.07	1.704

TABLE I: The values of  $c_D$  and  $c_E$  LECs for the Bochum  $N^3LO$  potentials with different cut-off parameters shown in the second column. In the  $N^3LO$  3NF relativistic  $1/m$  corrections and the  $2\pi$ -exchange-contact term were omitted.

cut-off	1	2	3	4
$\Lambda$ [MeV]	414	450	500	600

TABLE II: The values of the cut-off parameter  $\Lambda$  for the different  $N^3LO$  Idaho potentials.

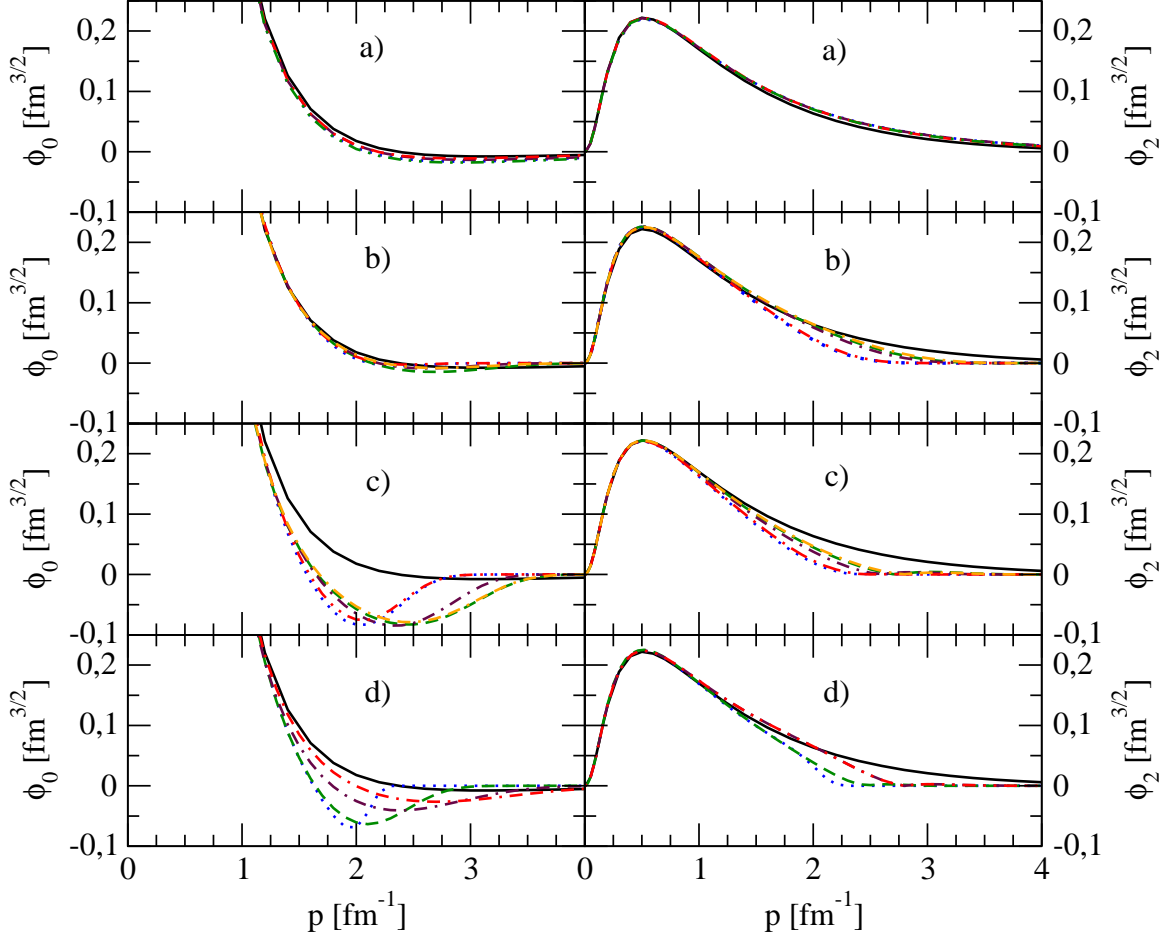


FIG. 9: (color online) The momentum space deuteron wave function for different NN potentials. The S- and D-components ( $\phi_0$  and  $\phi_2$ , respectively) are shown in the left and right columns, respectively. In a) wave functions for standard NN potentials are shown by different lines: AV18 - dotted (blue), CD Bonn - solid (black), Nijm 93 - dashed (maroon), Nijm I - dashed-dotted (red), and Nijm II - dashed-double-dotted (green). In b) and c) wave functions for the Bochum N<sup>2</sup>LO and N<sup>3</sup>LO NN potentials with different cut-off parameters from Table I are shown, respectively: (450,500) - dotted (blue) line, (600,500) - dashed (green) line, (550,600) - dashed-dotted (maroon) line, (450,700) - dashed-double-dotted (red) line, (600,700) - double-dashed-dotted (orange) line. The Idaho N<sup>3</sup>LO wave functions for different cut-off parameters from Table II are shown in d): 414 - dotted (blue) line, 450 - dashed (green) line, 500 - dashed-dotted (maroon) line, 600 - dashed-double-dotted (red) line. For comparison in b), c) and d) also the CD Bonn wave function is shown by solid (black) line.

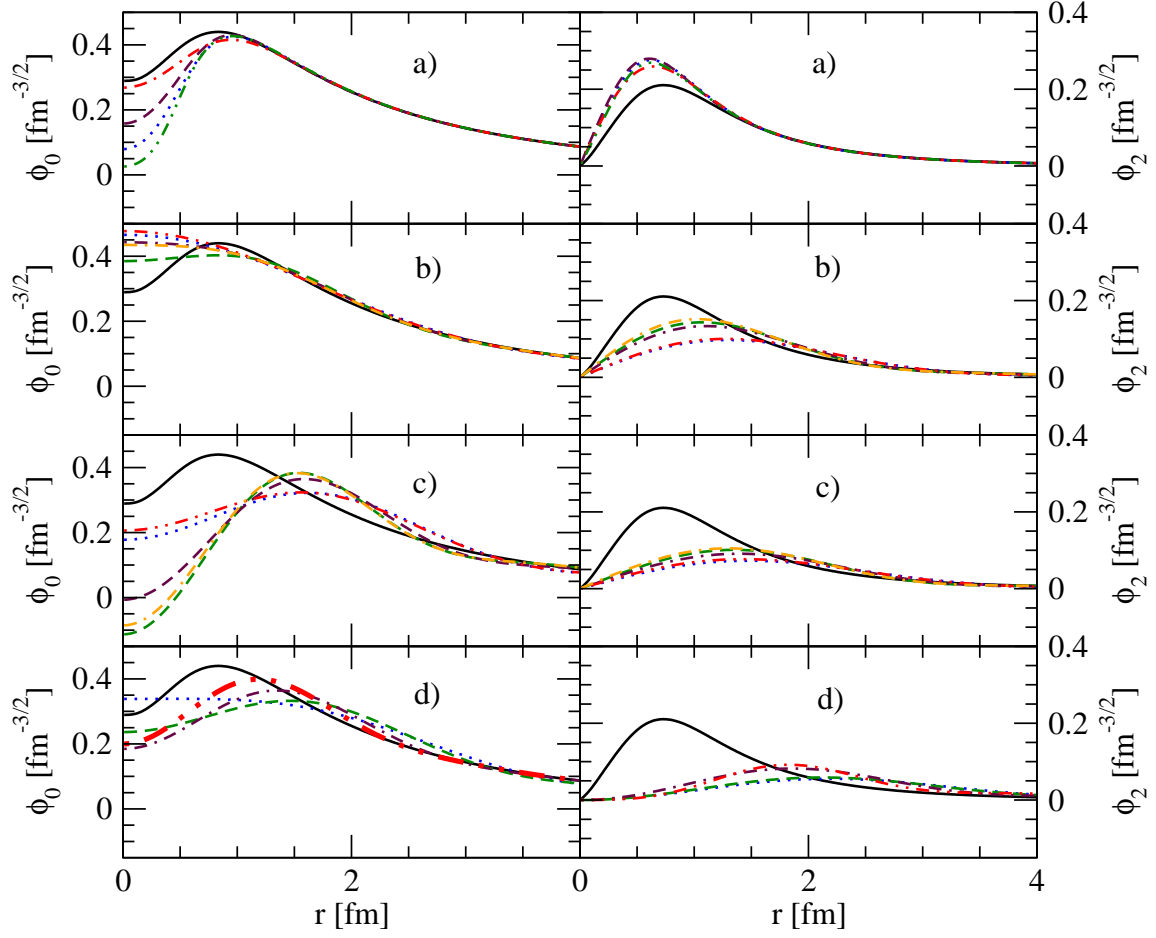


FIG. 10: (color online) The coordinate space deuteron wave function for different NN potentials. For explanation of lines see Fig.9.

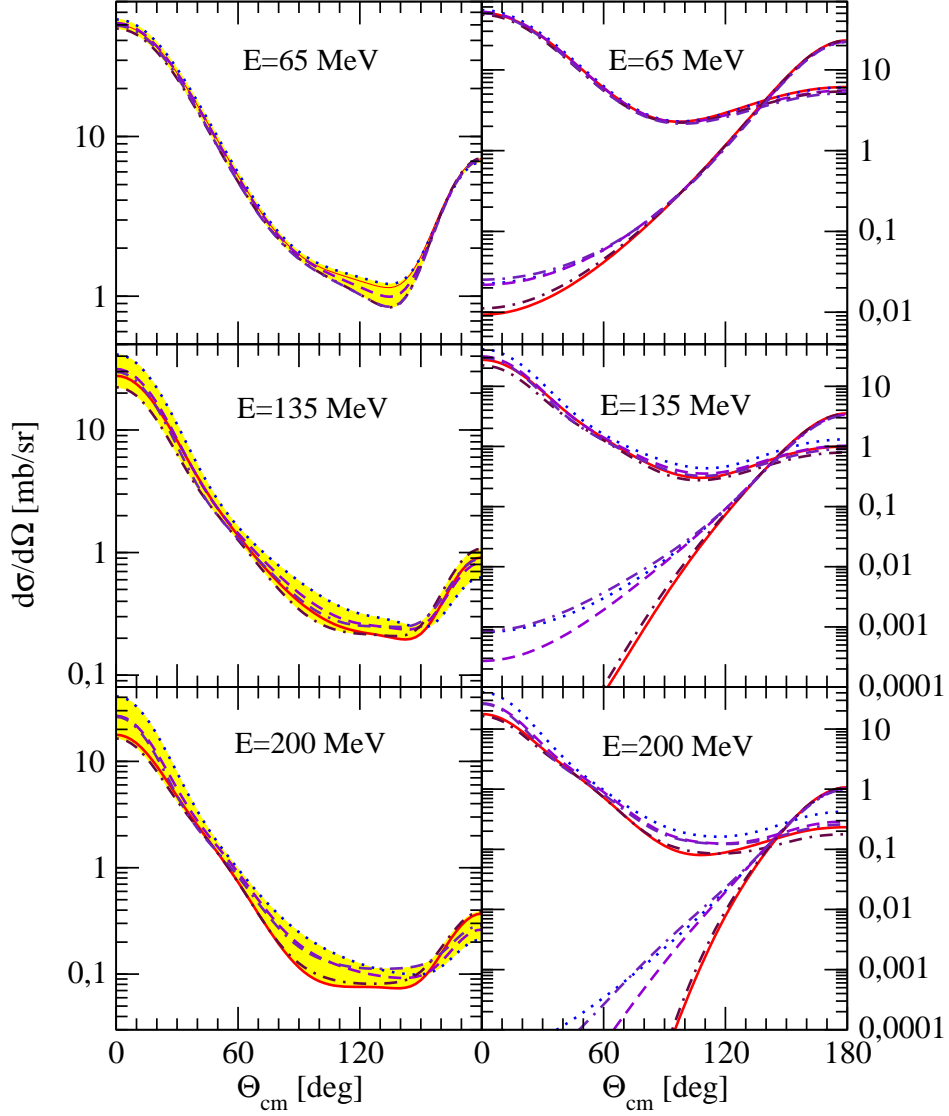


FIG. 11: (color online) The nd elastic scattering angular distributions at 65 MeV, 135 MeV and 200 MeV of incoming neutron lab. energy calculated with the Bochum  $N^2LO$  NN potentials for different cut-off values of Table I. In the left part the nd elastic scattering cross sections are shown. In the right part “cross sections” resulting only from the  $PT$  term in the elastic scattering transition amplitude are shown (lines peaked at forward angles) together with “cross sections” based on exchange-term  $PG_0^{-1}$  only (lines peaked at backward angles). Different lines correspond to different cut-off parameters from Table I: (450,500) - solid (red), (600,500) - dotted (blue), (550,600) - dashed (violet), (450,700) - dashed-dotted (maroon), (600,700) - double-dashed-dotted (indigo). In the left part light-shaded (yellow) bands show scatter of predictions for different cut-off values.

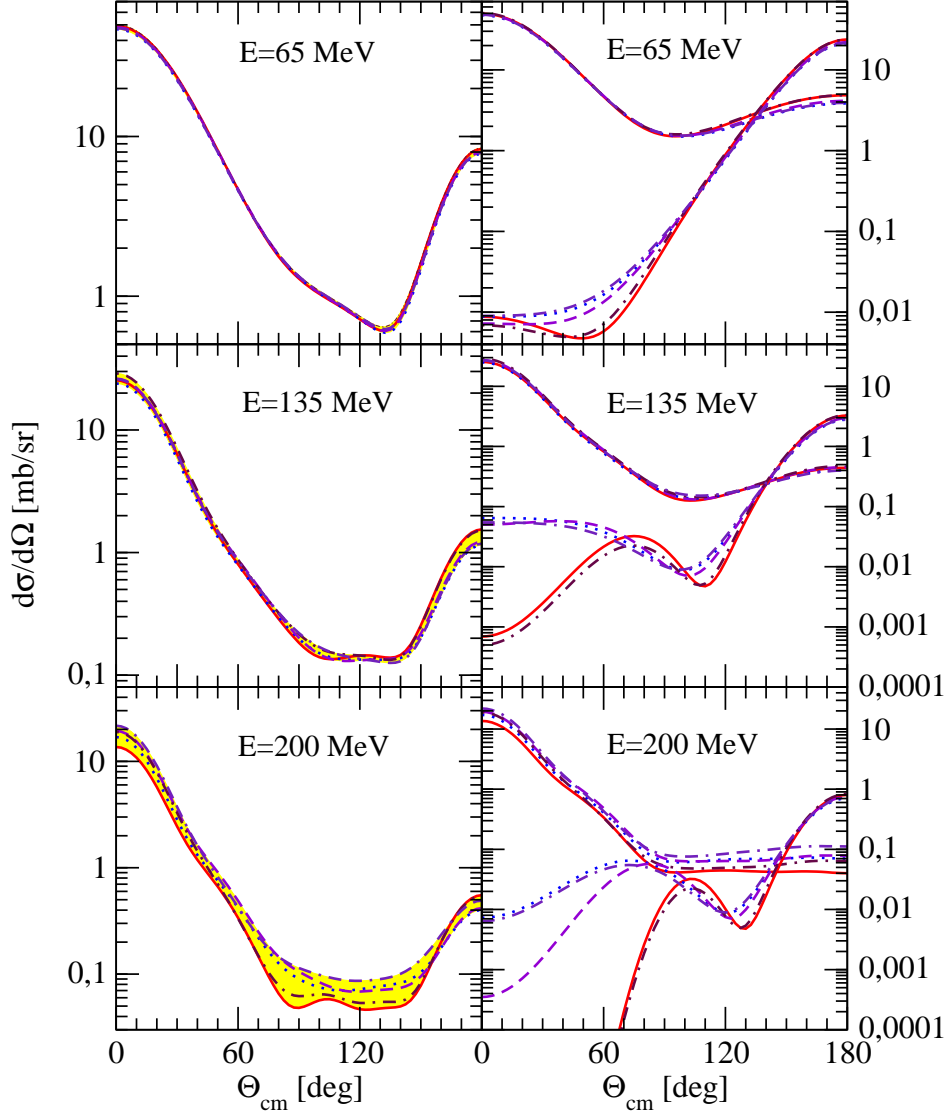


FIG. 12: (color online) The same as in Fig.11 but for the Bochum  $N^3LO$  NN potentials with different cut-off values of Table I. See Fig.11 for the description of lines and bands.

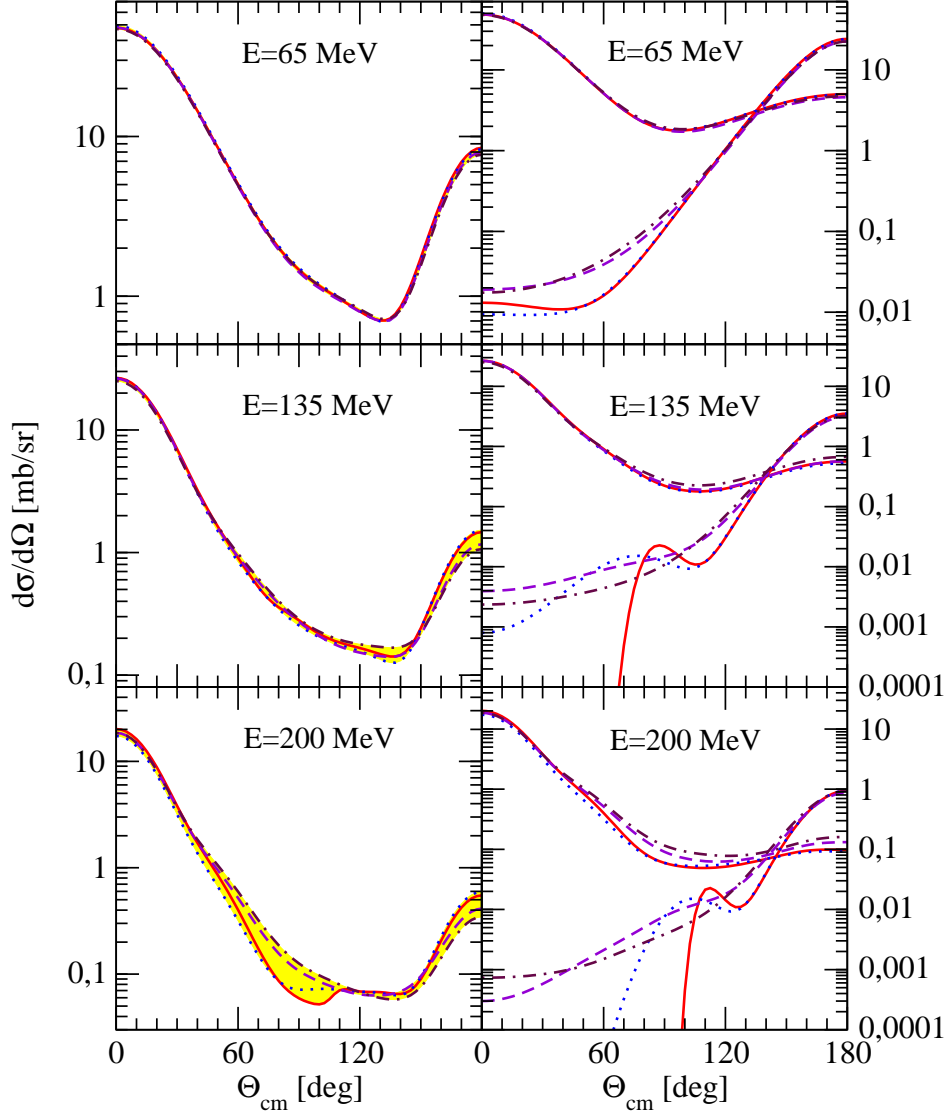


FIG. 13: (color online) The nd elastic scattering angular distributions at 65 MeV, 135 MeV and 200 MeV of incoming neutron lab. energy calculated with the Idaho  $N^3LO$  NN potentials for different cut-off values of Table II. In the left part the nd elastic scattering cross sections are shown. In the right part “cross sections” resulting only from the  $PT$  term in the elastic scattering transition amplitude are shown (lines peaked at forward angles) together with “cross sections” based on exchange-term  $PG_0^{-1}$  only (lines peaked at backward angles). Different lines correspond to different cut-off parameters from Table II: 414 - solid (red), 450 - dotted (blue), 500 - dashed (violet), 600 - dashed-dotted (maroon). In the left part light-shaded (yellow) band shows scatter of predictions for different cut-off values.